First-principles calculations of the electrical properties of LaAlO$_3$ and its interface with Si

A. A. Knizhnik,[1,*] I. M. Iskandarova,[1,2] A. A. Bagatur'yants,[1,3] B. V. Potapkin,[1,2] L. R. C. Fonseca,[4,†] and A. Korkin[5]

[1]*Kinetic Technologies Ltd, Kurchatov Square, 1, Moscow, 123182, Russia*
[2]*RRC "Kurchatov Institute," HEPTI, Kurchatov Square, 1, Moscow, Russia*
[3]*Photochemistry Center, Russian Academy of Sciences, ul. Novatorov 7a, 117421, Moscow, Russia*
[4]*Freescale Semiconductores Brasil Ltda, Jaguariúna 13820–000, Brazil*
[5]*Nano & Giga Solutions, 1683 East Spur Street, Gilbert, Arizona 85296, USA*
(Received 29 April 2005; revised manuscript received 27 October 2005; published 22 December 2005)

LaAlO$_3$ is one of the potential candidates to replace SiO$_2$ as a high permittivity dielectric for future generations of metal-oxide-semiconductor field effect transistors. Using first-principles plane-wave calculations within density functional theory, its bulk and surface electronic properties and the relative stability of cubic c-LaAlO$_3$(001)/Si(001) interfaces are investigated. In agreement with experiment, our study shows that the dielectric constant of crystalline LaAlO$_3$ ($\sim$30) is comparable to that of hexagonal La$_2$O$_3$. To accurately calculate the c-LaAlO$_3$(001) surface energy, several ways of eliminating the surface dipole moment of the polar surface are presented, with the transfer of an oxygen anion from one boundary surface to the other being identified as the energetically most favorable mechanism. We have found that lanthanum-terminated c-LaAlO$_3$(001)/Si(001) interfaces are in general more stable than aluminum-terminated interfaces for both the oxidized and nonoxidized Si(001) surfaces. We have also identified a significant reduction of the c-LaAlO$_3$(001)/Si(001) valence band offset due to the creation of interface dipoles for O-rich interfaces. Analysis of the density of interface states shows that La-Si bonds at the c-LaAlO$_3$(001)/Si(001) interface do not create interface states in the silicon band gap, in contrast to Hf-Si bonds in m-HfO$_2$(001)/Si(001) interfaces studied previously.

I. INTRODUCTION

The miniaturization of metal-oxide-semiconductor (MOS) technology has pushed the conventional SiO$_2$ gate dielectric close to its physical limit. For SiO$_2$ films thinner than $\sim$1 nm (physical thickness), direct tunneling through the dielectric barrier leads to unacceptably high leakage current.[1] Along with the difficulty to attain barrier thickness uniformity across the film, the resulting device performance and reliability are greatly reduced. To solve this problem high permittivity (high-k) dielectric materials, such as HfO$_2$, ZrO$_2$, and Y$_2$O$_3$,[1] have been proposed to replace SiO$_2$. However, many of these materials are not thermally stable on the silicon substrate: Either at deposition or during subsequent annealing treatments, the electrical properties of high-k films can suffer severe degradation due to interface reactions, ionic interdiffusion, or crystallization of as-deposited amorphous films.[1] Besides, the formation of an interfacial layer (IL) between the high-k film and the substrate due to oxidation of the substrate by excess oxygen in the bulk high-k film or during its initial stages of deposition causes a substantial reduction of the effective dielectric constant.[1] Recently much attention has been dedicated to HfO$_2$ because of its favorable electrical properties. However, Hobbs *et al.*[2] and Samavedam *et al.*[3] have shown that the interaction of HfO$_2$ with polysilicon and metal gates, respectively, can result in the pinning of the Fermi level, causing high threshold voltages. In addition, HfO$_2$ becomes polycrystalline during the processing temperature annealing, which may facilitate species diffusion through HfO$_2$ grain boundaries. The polycrystalline structure also creates a nonuniform dielectric along the channel length

with possible detrimental consequences to the electrical characteristics of the device. Therefore, it is of primary importance to consider alternative high-k candidates.

Recent experimental work has demonstrated that LaAlO$_3$ (LAO) is also a promising candidate for SiO$_2$ replacement due to its high-k value ($\sim$25), wide energy band gap ($\sim$5–6 eV), and thermal stability up to 2100 °C.[4,5] Moreover, LAO films on Si (Refs. 5 and 6) offer large band offsets for electron (1.8–2.0 eV) and hole (2.6–3.2 eV) tunneling. LAO films have been deposited on Si(001) substrates using chemical vapor deposition (CVD),[7] evaporation techniques,[8] and molecular beam epitaxy (MBE).[9,10] It was found that even in the amorphous phase, which is stable up to annealing temperatures of 800 °C, the dielectric constant of a thin LAO film remains quite large, $\sim$25. This value is close to that of La$_2$O$_3$ (LO) films;[11,12] however, LAO films are superior in thermal stability with respect to crystallization.[9,11]

The structure of the (001) surface of crystalline LAO was experimentally investigated in Refs. 13–18. It was suggested that the LAO surface termination depends on the temperature: For deposition at temperatures below 423 K, the surface is exclusively terminated by an Al-O layer, while at temperatures above 523 K the surface seems to be terminated by a La-O layer.[17,18] However, Francis *et al.*[13] have found that for temperatures ranging from room temperature to 670 K, the best fit to experimental data is attained assuming an aluminum-terminated surface, and that the surface undergoes significant structural relaxation at higher temperatures.

Only few theoretical studies describing the electrical properties of LAO films and interfaces have been published

so far. Jacobs *et al.* investigated the structure and relaxation of the LAO(001) surface using molecular dynamics based on empirical potentials.[19,20] They found that the AlO_2 termination, which can relax in a 5×5 surface reconstruction, is less stable than the LaO termination. Peacock and Robertson performed first-principles calculations of the LAO band structure.[21] Recently Wu *et al.*[22] and Delugas *et al.*[23] used density functional theory (DFT) to study the electric properties of LAO phases. In this work we report a first-principles investigation of the structure and electrical properties of bulk LAO and compare them with the corresponding properties of bulk LO. In addition, we study the preferential c-LAO(001)/Si(001) interface bonding and its impact on the band offset.

II. COMPUTATIONAL DETAILS

The structural and electrical properties of bulk LAO and c-LAO(001)/Si(001) (LAO/Si for simplicity) interfaces were investigated using the pseudopotential (PP)/DFT approach, with a basis set comprised of linear combinations of numeric pseudoatomic orbitals (LCAO) as implemented in the SIESTA code.[24] We also used a plane-wave (PW) basis set with the norm-conserving PPs as implemented in the ABINIT code[25,26] and with the ultrasoft PPs as implemented in the plane-wave self-consistent field (PWSCF) code.[27] In all the cases considered we used the local density approximation (LDA) with the Ceperley-Alder exchange correlation potential[28] within the Perdew-Wang parametrization.[29] In the PW calculations we used norm-conserving PPs of the Hartwigsen-Goedecker-Hutter form taken from Ref. 30 including semicore correction,[31] and ultrasoft PPs generated following the scheme described in Refs. 32 and 33 using the atomic configuration $[Kr\,4d^{10}]5s^25p^65d^16s^2$ for La. The norm-conserving PPs for LCAO calculations were of the Troullier-Martins (TM) type.[34] In this case, the La PP was generated for the neutral ground-state atomic configuration $[Kr\,5s^24d^{10}]4f^05p^65d^16s^2$ with the cutoff radii $r_s = 3.39$, $r_p = 1.48$, $r_d = 2.19$, and $r_f = 1.13$ bohr. The $5s$ electrons were treated as valence states. As to the other elements we used the neutral atomic ground-state configuration $[He]2s^22p^4$ for O with the cutoff radii $r = 1.14$ bohr for the s and p projectors, $[Ne]3s^23p^2$ for Si with the cutoff radii 1.89 bohr, and $[Ne]3s^23p^1$ for Al with the cutoff radii 2.28 bohr.

The LCAO calculations were performed using the single zeta plus polarization (SZP) numerical basis set including f orbitals for La. The Sankey-type numerical orbitals for La were constructed with the cutoff radii $r_s = 8.020$, $r_p = 4.083$, $r_d = 6.404$, and $r_f = 3.083$ a.u. (Ref. 24) using polarization functions for the $6s$ shell. We verified that the accuracy of this basis set is satisfactory by comparing the resulting lattice parameters and band structure with the values obtained with the double zeta plus polarization (DZP) and PW bases sets (see Table I and Fig. 1). We also found the impact of the f orbitals on the results of our calculations to be negligible.

The k-space sampling was obtained using a $7 \times 7 \times 7$ Monkhorst-Pack grid for bulk LAO, a $4 \times 7 \times 1$ grid for slabs with the 2×1 LAO surface unit, and a $4 \times 4 \times 1$ grid for the 2×2 LAO surface unit. The structures of all slabs

TABLE I. Structural parameters of c-LaAlO$_3$ and h-La$_2$O$_3$ calculated using different methods and the corresponding experimental data.

Parameter	SZP LCAO	DZP LCAO	PW	Experiment
		c-LaAlO$_3$		
a, Å	3.760	3.753	3.752	3.811[a]
B, GPa	243	239	217	
		h-La$_2$O$_3$		
a, Å	3.891	3.907	3.932	3.938–4.057[b]
c, Å	6.161	5.986	6.114	6.136–6.430

[a]Reference 35.
[b]Reference 36.

were fully optimized until the maximum residual force was less than 0.1 eV/Å.

Two methods were employed for the calculation of band alignment at the interface. First, we used projected density of states (PDOS) analysis[35] to estimate the valence band offset (VBO) from the results of the quantum mechanical calculations. We also applied the planar averaged potential (PAP) method of Van de Walle,[36] in which the electrostatic potential across the slab is calculated in conjunction with an additional bulk calculation for each material to obtain the VBO. We paid special attention to the convergence of the results as a function of the thickness of the Si and LAO slabs. We considered silicon and oxide thicknesses in the range 11–16 and 15–20 Å, respectively. The converged results presented here correspond to a stack composed of a LAO film $\sim$20 Å (five layers) thick and a Si film $\sim$12 Å (nine layers) thick.

III. RESULTS

A. Electrical properties of bulk LaAlO$_3$

Bulk LAO has a rhombohedral perovskite structure at room temperature and undergoes a transformation to a simple cubic structure at about 710–770 K.[37,38] This transformation involves changes in bond angles of only a tenth of a degree. In both phases the aluminum atoms occupy octahedral sites (AlO_6), while lanthanum atoms are 12-fold coordinated by oxygen atoms with equal bond lengths of about 2.70 Å. Since rhombohedral (r-LAO) and c-LAO phases have very similar structures we used c-LAO in our first-principles calculations of the electrical properties of bulk LAO and its interface with Si. Besides, current MOS technology requires annealing temperatures above 700 K,[1] which further justifies our choice of phase.

The optimized cell parameters of c-LAO and hexagonal LO (h-LO) calculated using the SZP and DZP LCAO, and PW bases sets are given in Table I together with the corresponding experimental data. The structural parameters of c-LAO were derived by fitting the calculated results to the Murnaghan equation of state[39] for both the PW and LCAO bases sets. Since c-LAO has cubic symmetry, its energy depends only on one parameter, the cell volume, and so the bulk modulus can be easily derived from the dependence of the cell energy on the cell volume. We found that the struc-
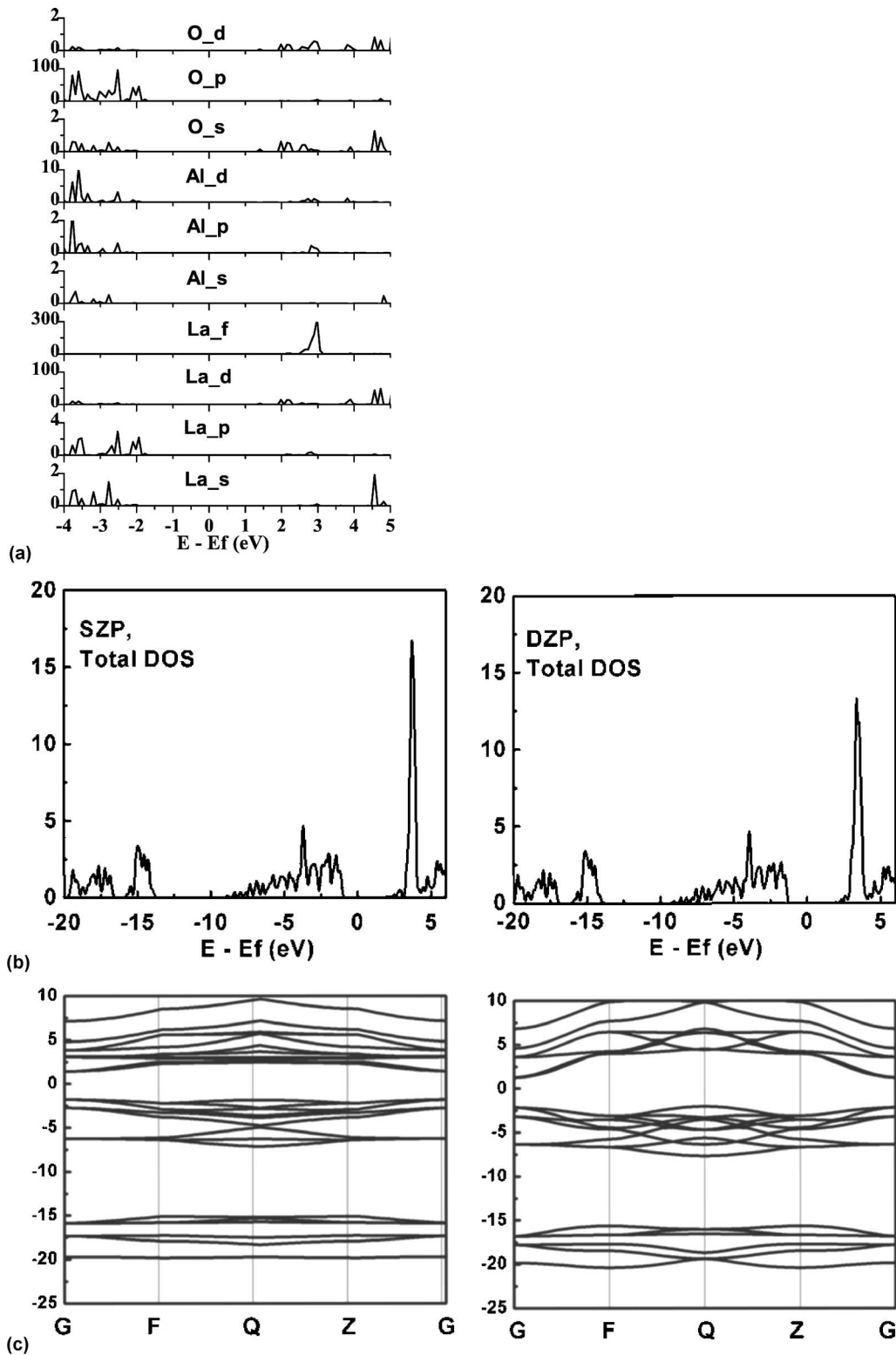
FIG. 1. Band structure and projected density of states (PDOS) of c-LaAlO$_3$ calculated with different bases sets: (a) PDOS (LCAO with SZP basis set); (b) total DOS with SZP and DZP LCAO bases sets; (c) band structures with SZP LCAO (top) and PW (bottom) bases sets.

tural properties of LAO and LO are reproduced quite accurately using the SZP LCAO basis, with a deviation from experimental data within the 1–2 % range. No significant improvement was obtained with the use of the enhanced DZP basis set. Moreover, the bulk modulus of c-LAO calcu-

lated using the SZP LCAO basis is within 10% of the PW result.

Figure 1 shows that the SZP and DZP basis sets give similar total density of states for c-LAO. It also demonstrates that the SZP LCAO and PW band structures for c-LAO dis-

TABLE II. Dielectric properties of h-La$_2$O$_3$, α-Al$_2$O$_3$ (included for comparison), and c-LaAlO$_3$ (experimental data from Ref. 1).

Structure	Exp. Gap (eV)	Calc. gap (eV)	Exp. ε	Calc. ε	Exp. ε_∞	Calc. ε_∞
LaAlO$_3$	5.6	3.3	23–27	29.7		4.7
La$_2$O$_3$	6.0	3.7	25	$\varepsilon_x=\varepsilon_y=21, \varepsilon_z=23$	4.0	4.8
Al$_2$O$_3$ (corundum)	8.8	4.6	12		3.4	

play the same features. The c-LAO conduction band is formed mainly by La d and f states, with the bottom of the band formed by d states and located at the gamma point of the Brillouin zone. The c-LAO valence band is formed mainly by O $2p$ electrons with the maximum of the band also located at the gamma point. Our calculations indicate that the band gap of c-LAO is narrower than that of h-LO (3.3 versus 3.7 eV in the PW/LDA/DFT approximation; see Table II). The band structure presented here for c-LAO is similar to that reported for rhombohedral LAO perovskite.[21]

The dielectric properties of c-LAO and h-LO were calculated using the PW/DFT approach. The linear response method[25,26] was used to calculate the effective charges, dielectric tensor, and phonon frequencies (Tables II–IV). The calculated low-frequency dielectric constant in c-LAO ($\varepsilon = 29.7$) is somewhat higher than that for h-LO ($\varepsilon_x=\varepsilon_y=21$, $\varepsilon_z=23$), while the high-frequency dielectric constants are almost identical for both crystals ($\sim$4.7 for c-LAO and $\sim$4.8 for h-LO). Note that the electrical properties of LAO are often measured for amorphous films and therefore can differ from the properties of the crystalline phase considered here. It is reasonable to assume that amorphous LAO has a smaller dielectric constant and a larger band gap than the crystalline phase: The reported LAO band gap for a single crystal film is 5.6 eV,[40] while it is 6.3 eV for the amorphous phase.[5] This fact explains why the calculated LAO dielectric constant is larger than measured values. The effective Born charges shown in Table III demonstrate that the La and O charge tensors in c-LAO and h-LO are quite similar. The calculated Born charges and phonon frequencies (see Table IV) for the c-LAO phase are in good agreement with those reported in Ref. 23. Our calculated Born charges are also quite close to the values calculated for r-LAO.[23] Nevertheless the DFT value for the orientation averaged a low-frequency dielectric constant of r-LAO (26) (Ref. 23) is lower than our value for c-LAO (29.7), showing that indeed the rhombohedral distortion can have a significant influence on the phonon frequencies and dielectric properties of LAO.[23]

B. Thermodynamic and electrical properties of LAO/Si interfaces
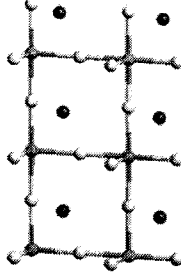
The stoichiometric LAO(001) slab is composed of alternating positively and negatively charged planes. The two slab surfaces contain charges of opp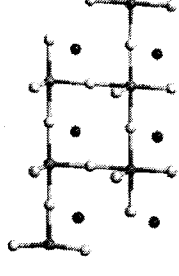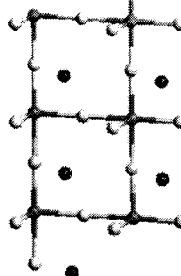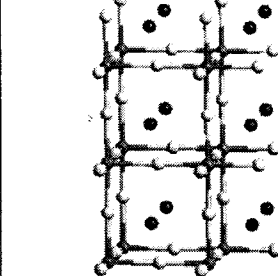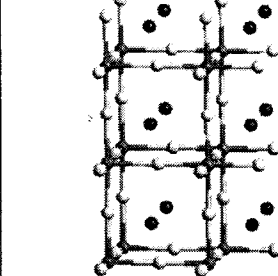osite sign, producing a net dipole perpendicular to the surfaces. Since the dipole moment depends on the separation between the surface charges it increases with the thickness of the slab causing an increase in the slab total energy.[41,42] This dipole-related divergence of the total energy can be removed using the technique commonly referred to as "metallization of polar surfaces",[42] but the residual electric field is too strong for the thin slabs considered in this work.[42] Therefore, we propose four possible ways to eliminate the slab dipole by transferring atoms from one side of the slab to the other. Table V shows the four cases: (a) transfer of one-half of the AlO$_2$ layer from one side of the LAO slab to the opposite side; (b) transfer of one-half of the LaO layer; (c) and (d) transfer of one oxygen atom from one side of the slab to the other. Even though slabs (c) and (d) are mirror reflections of each other along the normal direction to the surfaces, we still consider them as different structures since the two surfaces of each slab form different interfaces with Si. The energies of these LAO slabs in vacuum are given in Table VI showing that the most stable slabs correspond to configurations (c) and (d).

To study the thermodynamic and electrical properties of LAO/Si interfaces we constructed different interface configurations that were then optimized using LCAO/LDA/DFT calculations. We investigated four structures using the LAO slab models (a)–(d). For slab models (a) and (b), we considered symmetric (Si/LAO/Si) and asymmetric (Si/LAO) structures. For slab models (c) and (d) we considered only asymmetric (Si/LAO) structures since models (c) and (d) offer two different surfaces for building an interface with Si: The Si/LAO interface corresponding to model (c) involves the Al$_2$O$_3$ surface, while the interface corresponding to

TABLE III. Calculated effective Born charge tensors for c-LaAlO$_3$ and h-La$_2$O$_3$.

Structure			Charge
	La	Al	O
c-LaAlO$_3$	4.42	2.93	−2.45, −2.45, −2.45
h-La$_2$O$_3$	4.09		−2.74, −2.74, −2.51

TABLE IV. Calculated optical modes of cubic LaAlO$_3$ (all modes are threefold degenerated).

	Frequency (cm^{-1})	
Mode	This work	Reference 23
$F1_u$	168	167
$F2_g$	296	290
$F1_u$	414	412
$F1_u$	648	648

TABLE V. Standard LaAlO$_3$(001) slab with a nonzero net dipole moment (D), and LaAlO$_3$(001) slabs with modified surfaces (a)–(d) resulting in a zero net dipole moment.

Designation	Standard	(a) AlO$_2$ terminated	(b) LaO terminated	(c) O-shifted	(d) O-shifted
Structure	O La O La +1 Al O$_2$ Al O$_2$ −1 O La O La +1 Al O$_2$ Al O$_2$ −1 D ≠ 0!	Al O$_2$ O La O La Al O$_2$ Al O$_2$ O La O La Al O$_2$	O La Al O$_2$ Al O$_2$ O La O La Al O$_2$ Al O$_2$ O La	O O La O La Al O$_2$ Al O$_2$ O La O La Al O$_2$ Al O	Al O$_2$ Al O O La O La Al O$_2$ Al O$_2$ O La O La O

model (d) involves the LaO+O surface (see Fig. 2). We also considered interfaces with oxidized and unoxidized Si dimers (denoted by "Si-O-Si dimers" and "Si-Si dimers" in Table VI, respectively) on the Si(001) surface. The four different LAO/Si interfaces on the oxidized Si surface considered in this work are shown in Figs. 2(a)–2(d) (the unoxidized interfaces are identical to the structures shown in Fig. 2, except that the O atoms between Si atoms present in the oxidized cases are absent in the unoxidized cases). In addition to stoichiometric interfaces, we considered O-rich interfaces (labeled as "O-rich" in Table VI) constructed by adding an extra O atom to the interface area. The dangling bonds at the silicon slab/vacuum interface were saturated with hydrogen atoms.

The structural characteristics of the LAO/Si interfaces on the oxidized Si surface are shown in Fig. 2. The La atom at the interface forms two direct La-Si bonds 3.21 Å long, which is a typical length for La silicides.[43] Moreover, in the structure in Fig. 2(d) the transferred oxygen atom lies between Si-O-Si dimers at the distance 2.16 Å from two Si dimer atoms. The presence of the O atom between Si-O-Si dimers results in an increase of the Si-O dimer bond length from the typical value of 1.65 Å to the considerably larger value of 1.97 Å.

The calculated relative interface energies and VBOs are given in Table VI. The results show that the LaO termination is more favorable than the AlO$_2$ termination for all the interfaces considered. The interfaces depicted in Figs. 2(b) and 2(d) are the most stable for the stoichiometric LAO/Si interfaces with Si-O-Si dimers, with that shown in Fig. 2(d) being only slightly lower in energy. For the stoichiometric LAO/Si interfaces with Si-Si dimers, the interfaces depicted in Figs. 2(b) and 2(d) are also the most stable, with the interface in Fig. 2(b) being the lowest in energy. In case (b) we also placed a La atom above the Si-O-Si dimer but this structure

was 0.8 eV less stable, which is related to the repulsion between the La and O atoms in the dimers. The oxidation of Si-Si dimers is a favorable process for all four interfaces with average enthalpies of oxidation of about 3.0 eV per O atom. Table VI also shows that the VBOs calculated using the PAP method are in reasonable agreement with those found by the direct PDOS analysis technique and that the VBOs obtained with the LCAO and PW basis sets are quite similar, thus proving the accuracy of the LCAO approach for the system under consideration. The VBO results for models (a) and (b) in the asymmetric Si/LAO and symmetric Si/LAO/Si cases are slightly different, because the O2p states localized at the top LAO surface in the asymmetric Si/LAO interface can affect the VBO value. The difference between the VBOs calculated for the asymmetric Si/LAO and symmetric Si/LAO/Si slabs can be reduced by terminating the surface oxygen atoms in the asymmetric slabs with hydrogen atoms. Our calculations show that this procedure can fill empty surface states near Fermi level as shown in Fig. 3 for the structure given in Fig. 2(d), thus preventing Fermi level pinning by these states. However, the number of hydrogen atoms necessary to fully saturate the surface states is difficult to determine. Because of that, the symmetric Si/LAO/Si case should provide more relevant VBO results, and we used this case for the calculation of most VBO values in Table VI. On the other hand, the asymmetric Si/LAO slabs are better suited for calculations of relative energies of the deposited films (which have only one interface during oxide growth).

The incorporation of O atoms at the interface ("O-rich" case) strongly reduces the VBO due to the creation of an Si$^+$-O$^-$ interface dipole, which facilitates electron transfer from the oxide valence band to the Si substrate (see Ref. 44 for a detailed discussion). In this work, the charge transfer was obtained from Mülliken population analysis and is shown in Table VI, which displays the total charge of the Si

TABLE VI. Relative energies, valence band offsets, total charges on Si atoms, and enthalpies of oxidation reactions for the considered LAO/Si interfaces. All energies are in electron volts. Values in brackets are for the hydrogen termination of surface oxygen atoms in asymmetrical slabs.

Designation	(a) AlO$_2$ terminated	(b) LaO terminated	(c) O shifted	(d) O shifted
Slab structure	Al O$_2$ O La O La Al O$_2$ Al O$_2$ O La O La Al O$_2$	O La Al O$_2$ Al O$_2$ O La O La Al O$_2$ Al O$_2$ O La	O O La O La Al O$_2$ Al O$_2$ O La O La Al O$_2$ Al O	Al O$_2$ Al O O La O La Al O$_2$ Al O$_2$ O La O La O
Vacuum LAO slabs				
Relative energy	+2.42	+0.14	0.0	0.0
LAO/Si interfaces with Si-O-Si dimers				
LAO/Si				
Relative energy	+2.71	+0.06	+2.13	0.0
VBO (PDOS, LCAO/DFT)	1.5 (1.8)	0.9	0.9	2.1 (2.5)
VBO (PDOS, PW/DFT)	1.7	1.2		
Si/LAO/Si				
Relative energy	+2.66	0.0		
VBO (PDOS, LCAO/DFT)	1.75	1.0		
VBO (PAP, LCAO/DFT)	1.45	1.1		
Total charge in Si slab	2.89 e	2.01 e		
LAO/Si O-rich interfaces with Si-O-Si dimers				
Si/LAO/Si				
Relative energy	+4.75	0.0		
VBO (PDOS, LCAO/DFT)	1.0	0.2		
Total charge in Si slab	3.03 e	2.63 e		
LAO/Si interfaces with Si-Si dimers				
LAO/Si				
Relative energy	+2.10	−0.46	+1.25	0.0
VBO (PDOS, LCAO/DFT)	1.75	0.9	1.2	2.0
Enthalpy of oxidation reaction, E=E(Si-O-Si)−E(Si-Si)−E(O$_2$)/2	−3.38	−3.54	−2.26	−5.0
Si/LAO/Si				
Relative energy	+2.6	0.0		
VBO (PDOS, LCAO/DFT)	2.2	1.3		
Total charge in Si slab	2.22 e	1.54 e		

slab before and after O incorporation. The charge transfer obtained for the interface in Fig. 2(b) is significantly larger than that obtained for the interface in Fig. 2(a) due to the introduction of an oxygen atom mediating a La-Si bond, resulting in a stronger VBO reduction. For the unoxidized Si surface, no dangling bonds are present due to the formation of an additional π bonding by the Si-Si dimers. Therefore, the VBOs in this case are larger than for the oxidized Si surface.

Figure 4 shows the PDOS for all four interfaces calculated using the LCAO/DFT method. For interfaces (a) and (d) (see Fig. 2) with only Me-O (Me=La, Al) bonds at the interface, the Fermi level lies near the conduction band edge

(CBE) of Si. This is because the oxygen atoms in the oxide can be described as O^{2-} ions (with closed shells), thus pushing the Si dangling bond electrons up to the nearest unoccupied states, which correspond to the Si conduction band. For interface (b) the Fermi level lies in the middle of the Si band gap, because the extra Si dangling bond electrons can be accommodated by the states associated to La-Si bonds, which are located below the Si valence band edge (VBE) as shown in Fig. 4(b). Finally, for interface (c) the Fermi level lies at the Si VBE. In this case, all the interface bonds are of the Al-Si type with associated states near the Si VBE [Fig. 4(c)], which are partially occupied by one electron per Al-Si bond.
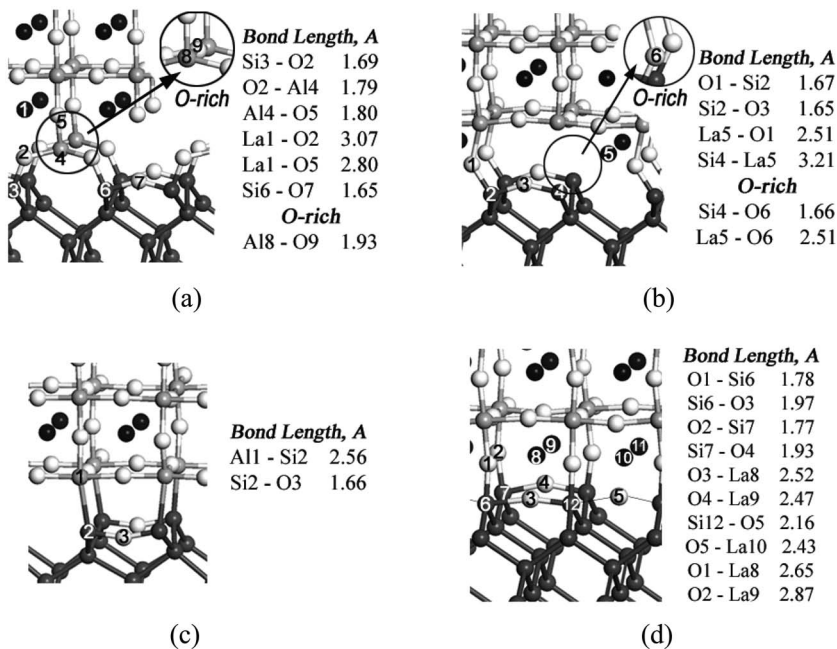
(a)

Bond Length, Å	
Si3 - O2	1.69
O2 - Al4	1.79
Al4 - O5	1.80
La1 - O2	3.07
La1 - O5	2.80
Si6 - O7	1.65
O-rich	
Al8 - O9	1.93

(b)

Bond Length, Å	
O1 - Si2	1.67
Si2 - O3	1.65
La5 - O1	2.51
Si4 - La5	3.21
O-rich	
Si4 - O6	1.66
La5 - O6	2.51

(c)

Bond Length, Å	
Al1 - Si2	2.56
Si2 - O3	1.66

(d)

Bond Length, Å	
O1 - Si6	1.78
Si6 - O3	1.97
O2 - Si7	1.77
Si7 - O4	1.93
O3 - La8	2.52
O4 - La9	2.47
Si12 - O5	2.16
O5 - La10	2.43
O1 - La8	2.65
O2 - La9	2.87

FIG. 2. $Si(001)/c$-$LaAlO_3(001)$ interfaces with bond distances (in angstroms) for the oxidized silicon substrate case (i.e., Si-O-Si on the Si surface). The notation (a)–(d) corresponds to that of Table V. Si: light gray; O: white; Al: dark gray; La: black. The position of an extra O atom in the corresponding O-rich interfaces is shown in the insets of (a) and (b).

The calculated VBOs using the PDOS approach for interfaces (a)–(d) are 1.5, 0.9, 0.9, and 2.1 eV (2.5 eV with hydrogen termination), respectively, smaller than the measured VBO value of 2.6–3.2 eV.[5,6] The first possible reason for such disagreement is that we have considered here only the crystalline phase of LAO, which has a smaller band gap [5.6 eV (Ref. 40)] than the amorphous phase [6.3 eV (Ref. 4)]. It is reasonable to expect the VBO for the crystalline phase to be also smaller than for the amorphous phase. Assuming that the VBO scales with the band gap [as already shown, this approximation yields good agreement between the measured and calculated VBOs (Ref. 45)], we can roughly estimate its value for the crystalline phase of LAO at approximately 2.3–2.8 eV, in good agreement with the 2.5 eV value that we calculated for the lowest energy interface (d) with interfacial Si-O-Si dimers and a hydrogen-saturated oxide surface. The second reason is the model character of our interface structures. Given the sensitivity of the VBO to the interface stoichiometry,[45,46] some level of disagreement should be expected. Finally, it is possible that the DFT/LDA prediction of VBOs [replacing the LDA functional by generalized gradient approximation (GGA) (Ref. 47) does not change the VBO by more than 0.1 eV] are incorrect as indicated by the GW-corrected calculations of the electronic structure of bulk ZrO_2.[48] The GW-corrected results show that the VBE decreases by approximately 1.2 eV with respect to the DFT value for tetragonal ZrO_2. Therefore the correction of the calculated band gap using the scissors operator (a shift of the CBE alone)[49] is incorrect for ZrO_2 and possibly for other oxides and metal/oxide interfaces as well, since the decrease of the oxide VBE may not be compensated by a shift of the metal Fermi level under GW. However, it is important to realize that while the GW shift of the oxide bulk VBE seems to correct the VBO, this procedure implicitly assumes that the charge transfer across the interface, which adds an energy step to the VBO (obtained in the Schottky limit of no interface pinning), is cor-
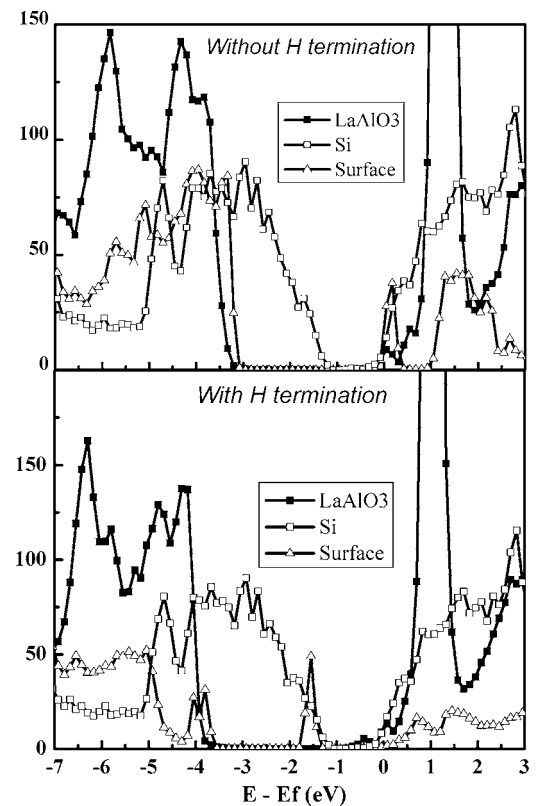

FIG. 3. DOS projected onto Si and c-$LaAlO_3$ atoms in the middle of the Si and c-$LaAlO_3$ slabs for the stack in Fig. 2(d) without (top) and with (bottom) hydrogen termination of the oxide surface. Additionally, DOS projected onto c-$LaAlO_3$ surface atoms showing a reduction of the density of empty surface states just above the Fermi level upon addition of hydrogen. The peak in the middle of the oxide band gap at -1.5 eV is associated with localized hydrogen states.
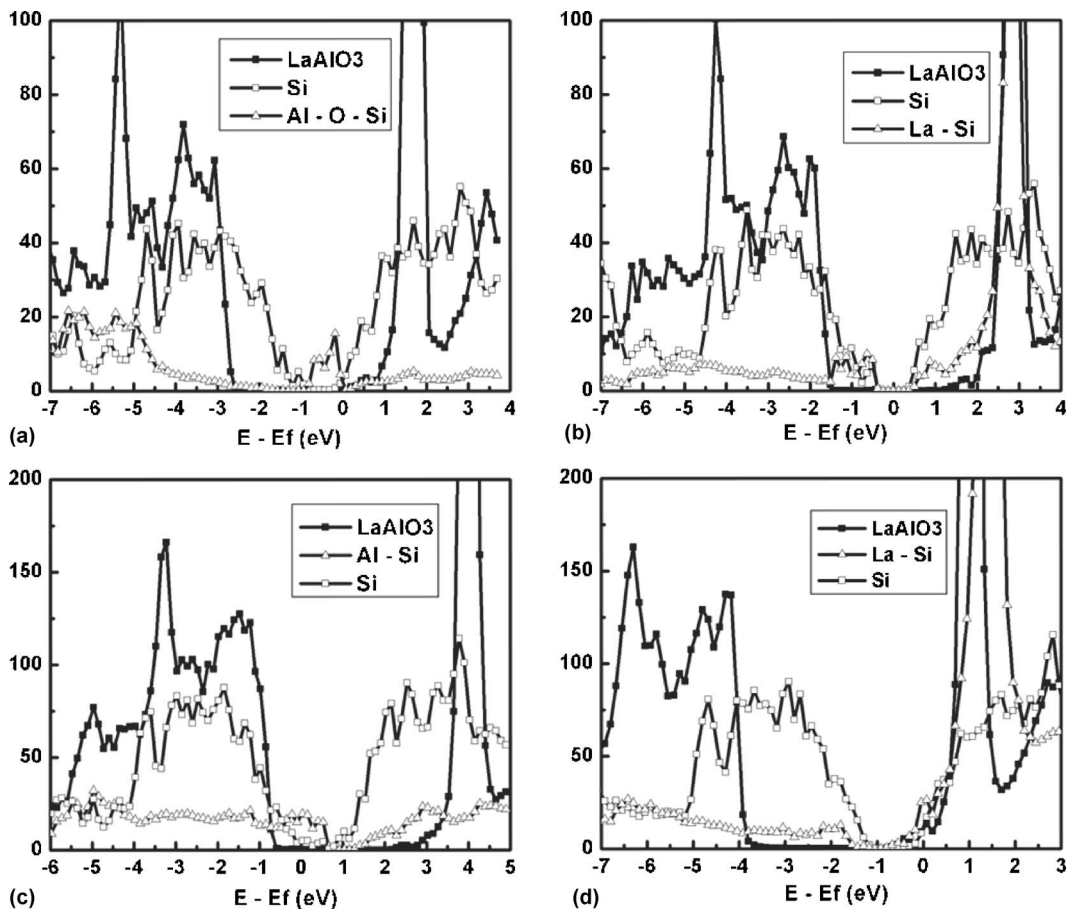
FIG. 4. (a)–(d) DOS projected onto Si and c-LaAlO$_3$ atoms in the middle of the Si and c-LaAlO$_3$ slabs for the stacks depicted in Figs. 2(a)–2(d), respectively. Additionally, DOS projected onto the Al–(O)–Si bonds (a), (c) and La–(O)–Si bonds (b), (d) at the c-LaAlO$_3$(001)/Si(001) interface. Notice the absence of states in the silicon band gap for interfaces (b) and (d). (The highest peak on the right side of each plot is related to the La $4f$ states introduced for completeness.)

rectly captured within DFT/LDA. If the interface dipole energy is also not accurate, then it will be necessary to consider an extension to the GW-derived VBO obtained from bulk calculations in order to accurately reproduce the experimental data.

Figure 4 also shows the PDOS obtained from the interfaces of the Si-LAO-Si symmetric structures [derived from Figs. 2(a) and 2(b)] and LAO-Si asymmetric structures [derived from Figs. 2(c) and 2(d)] with the oxidized Si dimers and H-saturated exposed oxide surface. It is interesting to note that La-Si bonds at the interface do not give rise to states in the Si band gap [Figs. 4(b) and 4(d)]. This fact does not depend on the oxidation of the silicon surface, thus the same picture is valid for the corresponding interfaces with unoxidized Si-Si dimers (not shown). On the other hand, Al-O-Si and Al-Si bonds at the interface result in a large density of states in the Si band gap [Figs. 4(a) and 4(c), respectively]. These gap states are partially occupied and are located approximately in the lower half of the Si band gap in the case of Al-Si bonds (mostly localized on the Si atom), whereas in the case of Al-O-Si bonds they are fully occupied (mostly localized on the O atom with a filled valence shell) and are located throughout the Si band gap. The penetration of these interface states in the LaAlO$_3$ and Si layers is shown

in Fig. 5 for the stack in Fig. 2(a). The penetration depth is about one LAO monolayer (3.8 Å) on the LAO side and about one Si monolayer (1.4 Å) on the Si side. The density of interface states is negligible farther away from the interface. The penetration depth in the LAO is in excellent agreement with the value of 3.6 Å obtained for bulk LO using complex band structure calculations of the spatial decay of the evanescent state at the charge neutrality level.[50]

These findings suggest that it is important to control the LAO deposition parameters to avoid or at least to ameliorate Fermi pinning at the LAO/Si interface in order to maximize both the VBO and CBO between LAO and the substrate or to reduce the threshold voltage in the case when polysilicon is used as gate metal.[2] It is desirable that the first layer in contact with Si is LaO (with a possible mix of La-O-Si and La-Si bonds at the interface) rather than AlO$_2$. This level of control may not be so difficult to achieve after all, since both LAO slabs and LAO/Si interfaces with LaO termination have the lowest energy (see Table VI). Therefore, it is possible that LAO/Si interfaces may display a smaller degree of Fermi pinning compared to the leading high-k gate dielectric under consideration, namely HfO$_2$ and its silicates and nitrides.[2]
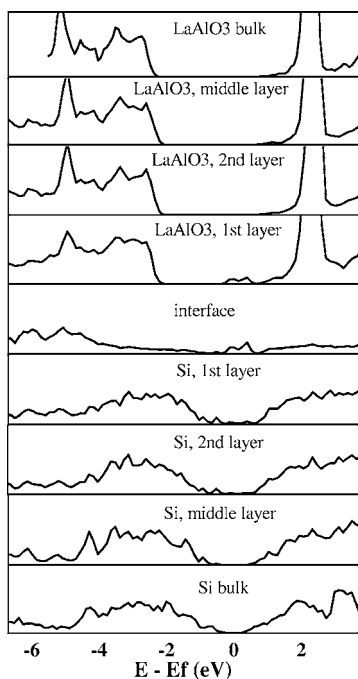
FIG. 5. DOS projected onto different Si and LaAlO$_3$ layers for the stack depicted in Fig. 2(a). The bulk DOS for LaAlO$_3$ is provided for comparison and is aligned to the LAO valence band edge.

IV. CONCLUSIONS

We have shown that the low-frequency dielectric constant of cubic LaAlO$_3$ (~30) is larger than that of hexagonal La$_2$O$_3$ (~22), while the high-frequency dielectric constant is comparable for the two materials. Concerning the stability of the LAO surface, in accordance with our calculations the most favorable way to compensate the LAO surface dipole is to transfer oxygen ions from one side of the slab to another, rather than formation of mixed La-Al layers. That is the case at least in the absence of OH adsorbed groups which can change the compensation mechanism as observed in the case of ZnO(0001),[51] for example. The presence of surface islands can also stabilize the mixed-layer dipole cancellation similar to the triangular structures observed on the ZnO(0001) surface.[51] However to our best knowledge islands have not been observed on the LAO(001) surface under the typical MOS processing temperature of 700 K.[1] So we can conclude that under such processing condition, the LAO surface should be either La or Al terminated, but not mixed, in agreement with experimental observations.[13,14]

For stoichiometric c-LaAlO$_3$(001)/Si(001) interfaces containing only metal-oxygen-silicon bonds at the interface, the closed-shell character of the oxygen anions in the oxide cause the promotion of the Si dangling bond electrons to the Si conduction band, placing the Fermi level at the Si conduction band edge. The crystallinity of the structures considered in this work, for which the experimental band gap [5.6 eV (Ref. 40)] is smaller than for the amorphous phase [6.3 eV (Ref. 5)], the sensitivity of the valence band offset to the interface atomic configuration, or possible limitations of the DFT/LDA approach may be responsible for the underestimation of the valence band offset, calculated in the 0.9–2.5 eV range [to be compared with the experimental value of 2.6–3.2 eV measured for amorphous LaAlO$_3$ on Si (Refs. 5 and 6)]. While the lowest energy interface considered has also the largest valence band offset calculated, 2.5 eV, scaling it by the ratio of crystalline to amorphous LAO band gaps yields an approximate valence band offset value of 2.8 eV, in better agreement with the experimental range. The incorporation of O atoms at the interface strongly reduces the VBO due to the creation of a Si$^+$-O$^-$ interface dipole. Finally, we found that while La-Si bonds at the c-LaAlO$_3$ interface with Si do not introduce states in the Si band gap, AlO$_2$ terminated interfaces do. These results suggest that in order to minimize Fermi pinning at the c-LaAlO$_3$(001)/Si(001) interface, processing steps should be taken to promote LaO as the first deposited monolayer on Si. Moreover, since LaO-terminated c-LaAlO$_3$ slabs and c-LaAlO$_3$(001)/Si(001) interfaces are lower in energy than the corresponding AlO$_2$-terminated structures, the c-LaAlO$_3$(001)/Si(001) interface may display a small degree of Fermi pinning without the need for complex interface engineering.

*Electronic address: knizhnik@kintech.ru

†Present address: Center for Semiconductor Components, Universidade Estadual de Campinas, Caixa Postal 6061, Campinas, SP 13083–870, Brazil. Electronic address: fonsecalrc@yahoo.com

[1] G. D. Wilk, R. M. Wallace, and J. M. Anthony, J. Appl. Phys. **87**, 484 (2000).

[2] C. C. Hobbs, L. R. C. Fonseca, A. Knizhnik, V. Dhandapani, S. B. Samavedam, W. J. Taylor, J. M. Grant, L. G. Dip, D. H. Triyoso, R. I. Hegde, D. C. Gilmer, R. Garcia, D. Roan, L. L. Lovejoy, R. S. Rai, E. A. Hebert, H.-H. Tseng, S. G. H. Anderson, B. E. White, and P. J. Tobin, IEEE Trans. Electron Devices **51**, 971/ 978 (Part 1/Part 2) (2004).

[3] S. Samavedam, L. B. La, P. J. Tobin, B. E. White, C. C. Hobbs, L. R. C. Fonseca, A. A. Demkov, J. Schaeffer, E. Luckowski, A. Martinez, M. Raymond, D. H. Triyoso, D. Roan, V. Dhandapani, R. Garcia, S. G. H. Anderson, K. Moore, H.-H. Tseng, and C. Capasso, *IEEE Int. Electron Devices Meeting*, Vol. 1, Proceedings of the IEDM (Washington D.C., 2003), p. 13.

[4] W. Xiang, H. Lu, L. Yan, H. Guo, L. Liu, Y. Zhou, G. Yang, J. Jiang, H. Cheng, and Z. Chen, J. Appl. Phys. **93**, 533 (2003).

[5] L. F. Edge, D. G. Scholm, S. A. Chambers, E. Cicerrella, J. L. Freeout, B. Hollander, and J. Schubert, Appl. Phys. Lett. **84**, 726 (2004).

[6] V. V. Afanas'ev, A. Stesmans, C. Zhao, M. Caymax, T. Heeg, J.

Schubert, Y. Jia, D. G. Schlom, and G. Lukovsky, Appl. Phys. Lett. **85**, 5917 (2004).

[7] M. V. Cabanas, C. V. Ragel, F. Conde, J. M. Gonzalez-Calbet, and M. Vallet-Regi, Solid State Ionics **191**, 101 (1997).

[8] B.-E. Park and H. Ishiwara, Appl. Phys. Lett. **79**, 806 (2001).

[9] B.-E. Park and H. Ishiwara, Appl. Phys. Lett. **82**, 1197 (2003).

[10] X. B. Lu, X. Zhang, R. Huang, H. B. Lu, Z. H. Chen, W. F. Xiang, M. He, B. L. Cheng, H. W. Zhou, X. P. Wang, C. Z. Wang, and B. Y. Nguyen, Appl. Phys. Lett. **84**, 2620 (2004).

[11] S. Stemmer, J.-P. Maria, and A. I. Kingon, Appl. Phys. Lett. **79**, 102 (2001).

[12] J.-H. Jun, C.-H. Wang, D.-J. Won, and D.-J. Choi, J. Korean Phys. Soc. **41**, 998 (2002).

[13] R. J. Francis, S. C. Moss, and A. J. Jacobson, Phys. Rev. B **64**, 235425 (2001).

[14] Z. L. Wang and A. J. Shapiro, Surf. Sci. **328**, 141 (1995).

[15] Z. L. Wang and A. J. Shapiro, Surf. Sci. **328**, 159 (1995).

[16] Z. L. Wang, Surf. Sci. **360**, 180 (1996).

[17] J. Yao, P. B. Merril, S. S. Perry, D. Marton, and J. W. Rabalais, J. Chem. Phys. **108**, 1645 (1998).

[18] P. A. W. van der Heide and J. W. Rabalais, Chem. Phys. Lett. **297**, 350 (1999).

[19] J.-P. Jacobs, M. A. S. Miguel, and J. E. Sanchez-Sanchez, J. Mol. Struct.: THEOCHEM **390**, 193 (1997).

[20] J.-P. Jacobs, M. A. S. Miguel, and J. E. Sanchez-Sanchez, Surf. Sci. **389**, L1147 (1997).

[21] P. W. Peacock and J. Robertson, J. Appl. Phys. **92**, 4712 (2002).

[22] S. A. Shevlin, A. Curioni, and W. Andreoni, Phys. Rev. Lett. **94**, 146401 (2005).

[23] P. Delugas, V. Fiorentini, and A. Filippetti, Phys. Rev. B **71**, 134302 (2005).

[24] J. M. Soler, E. Artacho, J. D. Gale, A. Garcia, J. Junquera, P. Ordejon, and D. Sanchez-Portal, J. Phys.: Condens. Matter **14**, 2745 (2002).

[25] X. Gonze, Phys. Rev. B **55**, 10337 (1997).

[26] X. Gonze and C. Lee, Phys. Rev. B **55**, 10355 (1997).

[27] S. Baroni, A. Dal Corso, S. de Gironcoli, and P. Giannozzi, http://www.pwscf.org

[28] D. M. Ceperley and B. J. Alder, Phys. Rev. Lett. **45**, 566 (1980).

[29] J. P. Perdew and Y. Wang, Phys. Rev. B **45**, 13244 (1992).

[30] C. Hartwigsen, S. Goedecker, and J. Hutter, Phys. Rev. B **58**, 3641 (1998).

[31] S. G. Louie, S. Froyen, and M. L. Cohen, Phys. Rev. B **26**, 1738 (1982).

[32] D. Vanderbilt, Phys. Rev. B **41**, R7892 (1990).

[33] K. Laasonen, A. Pasquarello, R. Car, C. Lee, and D. Vanderbilt, Phys. Rev. B **47**, 10142 (1993).

[34] N. Troullier and J. L. Martins, Phys. Rev. B **43**, 1993 (1991).

[35] A. A. Demkov, R. Lui, X. Zhang, and H. Loechelt, J. Vac. Sci. Technol. B **18**, 2338 (2000).

[36] C. G. Van de Walle and R. M. Martin, Phys. Rev. B **34**, 5621 (1986).

[37] S. Geller and V. B. Bala, Acta Crystallogr. **9**, 1019 (1956).

[38] H. M. O'Bryan, P. K. Gallager, G. W. Berkstresser, and C. D. Brandle, J. Mater. Res. **5**, 183 (1990).

[39] F. D. Murnaghan, Proc. Natl. Acad. Sci. U.S.A. **30**, 244 (1944).

[40] S.-G. Lim, S. Kriventsov, T. N. Jackson, J. H. Haeni, D. G. Schlom, A. M. Balbashov, R. Uecker, P. Reiche, J. L. Freeouf, and G. Lucovsky, J. Appl. Phys. **91**, 4500 (2002).

[41] M. S. Islam, Solid State Ionics **154**, 75 (2002).

[42] B. Meyer and D. Marx, Phys. Rev. B **67**, 035403 (2003).

[43] D. Gout, E. Benbow, and G. J. Miller, J. Alloys Compd. **338**, 153 (2002).

[44] A. Franciosi and C. G. Van de Walle, Surf. Sci. Rep. **25**, 1 (1996).

[45] L. R. C. Fonseca and A. A. Knizhnik (unpublished).

[46] A. A. Knizhnik, I. N. Iskandarova, A. A. Bagatur'yants, B. V. Potapkin, and L. R. C. Fonseca, J. Appl. Phys. **97**, 64911 (2005).

[47] J. P. Perdew, K. Burke, and M. Ernzerhof, Phys. Rev. Lett. **77**, 3865 (1996).

[48] B. Králik, E. K. Chang, and S. G. Louie, Phys. Rev. B **57**, 7027 (1998).

[49] Z. H. Levine and D. C. Allan, Phys. Rev. Lett. **63**, 1719 (1989).

[50] A. A. Demkov, L. R. C. Fonseca, E. Verret, J. Tomfohr, and O. F. Sankey, Phys. Rev. B **71**, 195306 (2005).

[51] G. Kresse, O. Dulub, and U. Diebold, Phys. Rev. B **68**, 245409 (2003).